fluorescence from platelets and leukocytes. Transdural observation can be less invasive in order to maintain natural condition of the brain.

Interaction of platelets and leukocytes may be induced by binding between P-selectin on the platelet surface and its ligand, PSGL-1 on the leukocyte surface. And this interaction would have some harmful effect on reperfusion injury on the brain. Color cranial window method applied to mice is very attractive to analyze the interaction of platelets and leukocytes on the brain.

References
1. Ishikawa M. et al. Stroke 34(7):1777-82, 2003.

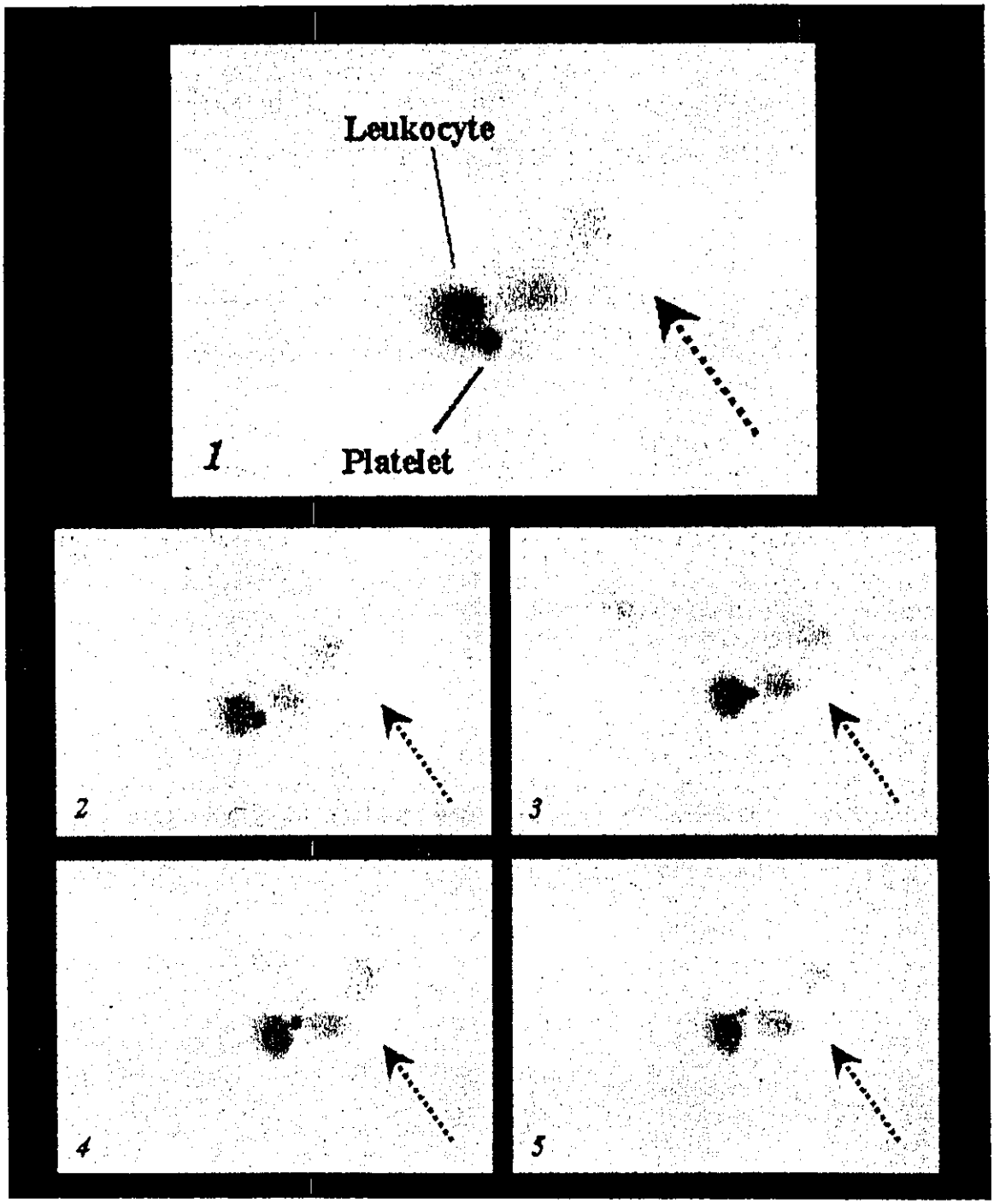

Fig. Sequential grayscale photographs of platelet rolling on the surface of sticking leukocyte. After adhering to the leukocyte surface, the platelet is moving downstream. (Dot arrow : blood stream)

(Key Word : ischemia, brain, reperfusion)

腎臓血管傷害のイメージング

国立感染症研究所生物活性物質部*，東京理科大学理工学部** 長尾 朋和*，村山 研*,**，越尾 修*
東京薬科大学薬学部#，東邦大学医学部大橋病院#* 大野 尚仁#，三浦 典子#，高橋 啓#*
オタゴ大学(ニュージーランド)† 馬渕 綾子†，南谷 晴之††
慶應義塾大学大学院基礎理工学部†† 鈴木 和男*,**

要 旨

腎炎，動脈炎，SLEなどの難治性血管炎は，好中球自己抗体(anti-neutrophil cytoplasmic antibodies；ANCA)が血清中に検出される自己免疫疾患で，免疫異常や好中球活性化と連動して進行するものと予想されている。好中球活性化の関与については，病理組織切片の観察の知見によっているが，生体ではどのような状況で活性化されているかは明らかではない。おそらく，*in vivo*での血管内部は，血管炎に伴って，血圧・血流速度などの血行力学的因子が変化していると想像される。これらの血流因子の変化を*in vivo*で解析し，血管傷害の要因を検証することが必要である。この方法には，顕微鏡を用いた*in vivo*の生存状態で，臓器微小循環血流を観察して，血流のパラメーターを定量的に評価することが必要である。この方法により，腎炎において重要な働きを担っているものと思われる好中球の動態も*in vivo*での観察・解析が可能である。そこでわれわれは，腎炎の発症・進展におけるANCAおよび好中球の役割を明らかにするために，腎炎モデルマウスの構築およびin vivoイメージング観察を行った。その結果，*Candida albicans*由来糖ペプチド(CAWS)，rabbit anti-mouse myeloperoxidase(anti-mMPO)およびfMet-Leu-Pheによって腎血管傷害を誘導したC57BL/6マウスでは，血流速度の低下，血流停止，血液の逆流などが観察され，最も顕著な場合，広範囲にわたる腎表面血流の停止も観察された。さらに，これらの現象には血管内皮への白血球の接着も観察された。本腎炎誘導モデルにおいては，myeloperoxidase(MPO)が関連していることから，観察された白血球のなかでも特に好中球が炎症における重要な役割を担っているものと考えられる。本血管炎誘導モデルにおいて開発したin vivoイメージングの評価法は，血管炎の進行によって誘発される多臓器不全の治療法の開発や，治癒機転および発症機構を解析するうえで有用であることを示した。

I. 緒 言

難治性血管炎は，腎炎，動脈炎やSLEなどとして顕れ，その要因の1つにANCAが，血清中に増加することが明らかにされてきている[1)-4)]。このように，難治性血管炎には，自己免疫疾患などの免疫異常が関与している[5)]。また，ANCAの対応分子の主なものが，好中球顆粒酵素のprotease-3(PR-3)やMPOであることから，好中球の活性化が発症や病態に関与していることが予想される[6)7)]。

また，生体防御機能の不全は，好中球や免疫細胞の機能破綻やそれによるサイトカインの異常なネットワークのかく乱を誘導し，種々の臓器障害をもたらす。血管内皮細胞は，サイトカインと活性化白血球の攻撃にさらされ，また，臓器内での異常反応の前線となる。特に，好中球活性化は，難治性血管炎の発症およびその要因になっていることが強く示唆されており，好中球の殺菌酵素であるMPOがMPO-ANCAの抗原になっていることをわれわれは明らかにした[8)]。すなわち，ANCAが好中球を活性化し，血管炎の発症に関わっている可能性を示唆した[9)10)]。

一方，血管炎の病初期には，病理組織切片の観察から好中球が浸潤していることから裏付けられている。しかし，病理所見による*in vitro*の観察は，生体の生きたままでの観察ではないことから，生体での状況をそのまま解析することはできない。血管炎に伴って，生体の血管内部では，血圧・血

流速度などの血行力学的因子が変化していると推定されるが，*in vitro*では，これらの因子の変化をとらえることはかなり困難である。しかしながら，これらの因子が血管傷害に影響を及ぼすかを検証することが必要である。そこで，顕微鏡を用いた*in vivo*の観察システムより，生存状態で臓器微小循環血流を観察して，これらのパラメーターを定量的に評価することが必要である。さらに，重要な働きを担っているものと推定されている好中球の血管内部での動態も，本システムを使って*in vivo*での観察・解析をすることも重要である。一方，本システムの開発には，動物モデルが必要である。そこで，カンジダ菌成分Candida albicans derived substances (CADS)の接種による好中球抗体MPO-ANCAが血中に増加する冠状動脈炎モデルを用いた[11]。また，カンジダ菌外成分CAWSも血管炎を強く誘導することが可能である。

そこで，本研究では，CAWSによる腎傷害モデルマウスを作製し，本モデルマウスにより，in vivoイメージング法を開発した。それにより，腎炎の発症・進展におけるANCAおよび好中球の役割を検討した。

Ⅱ．研究方法

①多臓器不全関連血管炎モデルマウスの調整：*C. albicans*由来物質CAWSを投与して誘導した。

②in vivo イメージング：C57BL/6マウス(オス，9週齢)にCAWS(150 mg/mouse)をiv投与し，3時間後にanti-mMPO(rabbit anti-mouse myeloperoxidase，1 mg/mouse)をiv投与した。5日後，同様にCAWSとanti-mMPOを投与した後，fMet-Leu-Phe(FMLP，10^{-8} mol/mouse，細菌由来トリペプチド)をiv投与し，その3日後に腎表面における血流状態を観察した。血流の可視化にはFITC-dextranを用い，各マウスの腎表面における尿細管周囲毛細血管の血流を観察した。観察される血流動態は顕微鏡に接続したビデオカメラで撮影し，DVDに録画した。

Ⅲ．結　果

腎血管傷害を誘導するためにCAWS，anti-mMPOおよびfMet-Leu-Pheを投与し，腎臓表面血管のin vivoイメージングにより，血流速度の低下，血流停止，血液の逆流を観察・解析した。

①PBS投与のコントロールマウスでの腎臓血管の血流を観察した(図1)。

図1．コントロールマウスの腎血管のin vivoイメージング

②CAWS，anti-mouseMPOおよびfMet-Leu-Pheの投与による腎微小循環傷害のin vivoイメージング。

CAWS，anti-mouseMPOおよびfMet-Leu-Pheの投与によって，腎微小循環が悪化する様子がin vivoイメージングにより観察された(図2)。CAWSの投与によって，冠状動脈炎が誘導された。その頻度は，100%近い値を示した。この濃度以上の投与は，全身性の多臓器不全様ショックにて死亡した。また，in vivoイメージングの解析では，血流速度の低下，血流停止，血液の逆流が観察され，腎表面血流の停止がみられた(図2)。

③血流遮断と血管内皮細胞への白血球接着。

腎臓表面血管の流速の変化も，CAWS＋anti-mouseMPO＋fMet-Leu-Pheのときに悪化した。血流速度の低下・血流停止・血液の逆流などの現象が観察され，CAWSまたはFMLP単独投与の場合と比較し，両者に加えてanti-mMPOを投与した場合に血流停止が誘発され(観察した血管の約10%)，広範囲にわたる腎表面血流の悪化が観察された(約30%)。さらに，この腎微小循環の悪化には血管内皮細胞への白血球の接着を伴ったものもみられた(図3)。

C57BL/6マウスにCAWS，anti-mMPOおよびfMet-Leu-Pheを投与して誘導される腎血管傷害をin vivoイメージングにより，血流速度の低下，血流停止，血液の逆流を観察した。また，広範囲にわたる腎表面血流の停止も観察した。さらに，これらの現象には血管内皮への白血球の接着を伴ったものも観察された。

Ⅳ．考　察

CAWSによって，冠状動脈炎が100%近く発症し，投与量の増加により，多臓器不全様ショックで死亡した。この血管炎誘導モデルにおいては，*C. albicans*由来糖ペプチドCAWSが，MPOおよびMPO-ANCA産生と発症誘導に不可欠であることから，CAWSなどの真菌由来分子がサイトカインと連動して好中球を活性化して，多臓器不全様の症状を誘発する役割を担っているものと考えられる。その結果，急速な血管炎を誘発し，ひいては，多臓器不全をきたしたと考えられる。そのCAWSに加え，anti-mouseMPOおよびfMet-Leu-Pheを投与し，in vivoイメージングすることにより，血流速度の低下，血流停止，血液の逆流が観察され，腎表面血流の停止や血管内皮への白血球の接着も

図2．CAWS誘導の腎血管傷害in vivoイメージング
CAWS＋anti-mMPO＋FMLP

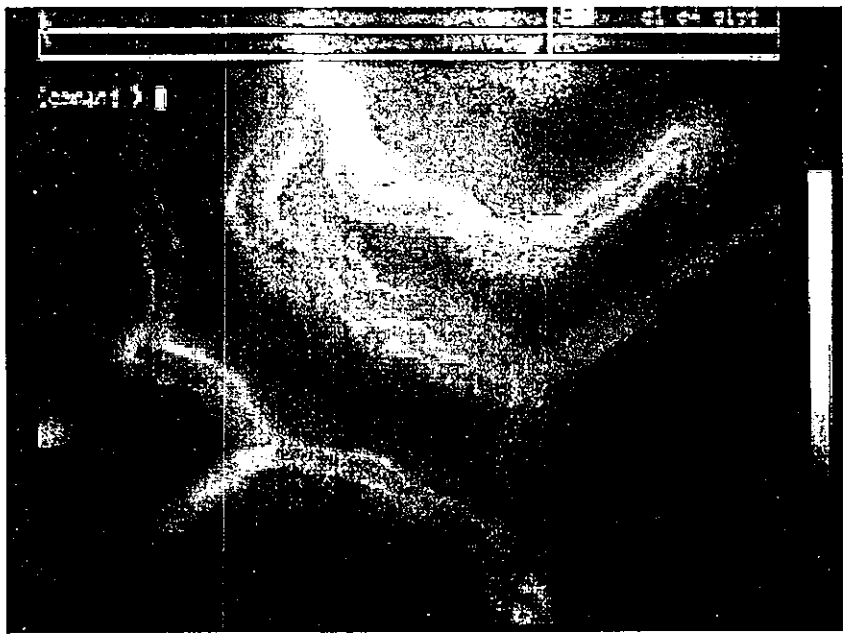

図3．CAWS誘導の腎血管傷害in vivoイメージングにおける血管内皮への白血球の接着

みられた。この*in vivo*での現象が，腎血管傷害の誘導を説明できると思われるが，分子機構との関係を明らかにする必要があり，さらに検討する必要がある。CAWSおよびanti-mMPOによって誘導される腎微小血管傷害誘導モデルを用いたin vivoイメージングの解析から以下のような推論が得られた。まずCAWSによって好中球数の増加・好中球活性化が誘発される。この状態において投与された好中球自己抗体(anti-mMPO)は，活性化によって細胞膜表面へ移行したMPOと複合体を形成し，さらなる好中球の活性化・血管内皮細胞への接着・活性酸素種の産生を引き起こすと考えられる。このことから，白血球のなかでも特に好中球が炎症における重要な役割を担っているものと推察される。また，このin vivoイメージング解析による評価法は，CAWS誘導血管炎やSCG/Kjマウスなどの腎炎モデル[12)-14)]での発症機構の解析に有用であり，本システムの利用が期待される。また，血管炎の治療法[15)-17)]の新しい評価系として有用であると思われる。このように，微小血管傷害を生体内で観察するシステムは，血管炎や多臓器不全の治療法の評価や治癒機構の解析として，今後の利用が期待される。

文　献

1) Jennette JC, Falk RJ：Antineutrophil cytoplasmic autoantibodies and associated diseases：a review. Am J Kidney Dis 15：517−529, 1990
2) Suzuki K：Neutrophil functions of patients with vasculitis related to MPO-ANCA. Int J Hematol 74：134−143, 2001
3) Savage COS, Winearls CG, Jones SJ, et al：Prospective study of radioimmunoassay for antibodies against neutrophil cytoplasm in diagnosis of systemic vasculitis. Lancet 1：1389−1393, 1987
4) Cohen Tervaert JW, Goldschmeding R, Elema JD, et al：Autoantibodies against myeloid lysosomal enzymes in crescentic glomerulonephritis. Kidney Int 37：799−806, 1990
5) Harper JM, Thiru S, Lockwood CM, et al：Myeloperoxidase autoantibodies distinguish vasculitis mediated by anti-neutrophil cytoplasm antibodies from immune complex disease in MRL/Mp-lpr/lpr mice：a spontaneous model for human microscopic angitis. Eur J Immunol 28：2217−2226, 1998
6) Tomizawa K, Mine E, Fujii A, et al：A panel set for epitope analysis of myeloperoxidase (MPO)-specific antineutrophil cytoplasmic antibody MPO-ANCA using recombinant hexamer histidine-tagged MPO deletion mutants. J Clin Immunol 18：142−152, 1998
7) Fujii A, Tomizawa K, Arimura Y, et al：Epitope analysis of myeloperoxidase (MPO) specific anti-

neutrophil Cytoplasmic autoantibodies (ANCA) in MPO-ANCA-associated glomerulonephritis. Clin Nephrol 53：242－252, 2000
8) Ishida-Okawara A, Oharaseki T, Takahashi K, et al：Contribution of myeloperoxidase to coronary artery vasculitis associated with MPO-ANCA production. Inflammation 25：381－387, 2001
9) 鈴木和男：血管炎発症機構の解析研究-活性化好中球の関与. 医学のあゆみ 206：133－139, 2003
10) 鈴木和男：ANCA関連血管炎の発症機序-活性化好中球の関与. リウマチ科 29：228－236, 2003
11) Murata H, Iijima H, Naoe S, et al：The pathogenesis of experimental arteritis induced by Candida alkali-extract in mice. Jpn J Exp Med 57：305－313, 1987
12) Kinjoh K, Kyogoku M, Good RA：Genetic selection for crescent formation yields mouse strain with rapidly progressive glomerulonephritis and small vessel vasculitis. Proc Natl Acad Sci USA 90：3413－3417, 1993
13) Cherry Engelman RW, Wang BY, Kinjoh K, et al：Calorie restriction delays the crescentic glomerulonephritis of SCG/Kj mice. Proc Soc Exp Biol Med 218：218－222, 1998
14) Ishida-Okawara A, Ito Ihara T, Muso E, et al：Neutrophil contribution to the crescentic glomerulonephritis in SCG/kj mice. Nephrol Dial Transplant (in press)
15) Jayne DR, Chapel H, Adu D, et al：Intravenous immunoglobulin for ANCA-associated systemic vasculitis with persistent disease activity. QJM 93：433－439, 2000
16) Jayne DR：Update on the European Vasculitis Study Group trials. Curr Opin Rheumatol 13：48－55 (Review), 2001
17) Ito-Ihara T, Nogaki F, Ono T, et al：Intravenous immunoglobulin (IVIG) treatment of MPO-ANCA-related microscopic polyangiitis. Cleveland Clin J Med Suppl 69：SII－188, 2002

J Appl Physiol 96: 1561–1568, 2004.
First published December 5, 2003; 10.1152/japplphysiol.00764.2003.

HIGHLIGHTED TOPIC | *Oxygen Sensing in Health and Disease*

Red blood cell velocity and oxygen tension measurement in cerebral microvessels by double-wavelength photoexcitation

Kosuke Tsukada,[1] Eiichi Sekizuka,[2] Chikara Oshio,[3] Katsuhiko Tsujioka,[1] and Haruyuki Minamitani[4]
[1]*Department of Physiology, Kawasaki Medical School, Kurashiki, 701-0192;*
[2]*Department of Clinical Research, National Saitama Hospital; Wako, 351-0102;* [3]*Oshio Clinic, Chiyoda-ku, 101-0063; and* [4]*Department of Applied Physics and Physico-Informatics, Faculty of Science and Technology, Keio University, Yokohama, 223-8522 Japan*

Submitted 23 July 2003; accepted in final form 2 December 2003

Tsukada, Kosuke, Eiichi Sekizuka, Chikara Oshio, Katsuhiko Tsujioka, Haruyuki Minamitani. Red blood cell velocity and oxygen tension measurement in cerebral microvessels by double-wavelength photoexcitation. *J Appl Physiol* 96: 1561–1568, 2004. First published December 5, 2003; 10.1152/japplphysiol.00764.2003.—Because the regulation of microcirculation in the cerebral cortex cannot be analyzed without measuring the blood flow dynamics and oxygen concentration in cerebral microvessels, we developed a fluorescence and phosphorescence system for estimating red blood cell velocity and oxygen tension in cerebral microcirculation noninvasively and continuously with high spatial resolution. Using red blood cells labeled with fluorescent isothiocyanate to visualize red cell distribution and using the oxygen quenching of Pd-meso-tetra-(4-carboxyphenyl)-porphyrin phosphorescence to measure oxygen tension enabled simultaneous measurement of blood velocity and oxygen tension. We examined how the measurement accuracy was affected by the spatial resolution and by the excitation laser light passing through the targeted microvessel and exciting the oxygen probe dye in the tissue beneath it. Focusing the excitation light into the microvessel stabilized the phosphorescence lifetime at each spatial resolution; moreover, it greatly reduced phosphorescence from the brain tissue. Animal experiments involving acute hemorrhagic shock demonstrated the feasibility of our system by showing that the changes in venular velocity and oxygen tension are synchronized to the change in mean arterial pressure. Our system measures the red cell velocity and oxygen concentration in the cerebral microcirculation by using the differences in luminescence and wavelength between fluorescence and phosphorescence, making it possible to easily acquire information about cerebral microcirculatory distribution and oxygen tension simultaneously.

cerebral microcirculation; erythrocyte velocity; oxygen tension; fluorescence; phosphorescence

THE CEREBRAL NERVE CELLS ARE extremely vulnerable to ischemia because they store hardly any oxygen or substrates. Because higher brain function therefore depends on the microcirculation, the brain is expected to have a strong autoregulation maintaining the local blood flow and volume. Consequently, an extremely effective way to study the regulation of the microcirculation in the cerebral cortex is by measuring the dynamics of the cerebral microcirculation while simultaneously measuring the oxygen concentration in the cerebral microvessels.

When one measures the microcirculatory blood flow in two-dimensional structures such as dorsal skin, the mesentery or cremaster muscle, the cheek pouches of hamsters, and the ears of rabbits, one can observe these structures under transmitted illumination. Although the microcirculation in the brain cortex cannot be observed under transmitted illumination, the dynamics of the blood flow distribution can be visualized by using FITC-labeled red blood cells (RBCs) and an incident-light fluorescence microscope, as described by Ishikawa et al. (3). On the other hand, the oxygen electrodes often used when measuring oxygen tension in vivo cannot be used in microvessels because they physically damage them too much and because their spatial resolution is inadequate. The partial pressure of oxygen in organs must therefore be measured by a noncontact, noninvasive method. The oxygen tension can be measured in vivo by using the changes in the lifetime of phosphorescence emitted from a porphyrin dye, as reported (12, 22), and this technique is being established as an alternative method for measuring the oxygen tension in organs.

In the present study, we used fluorescently labeled RBCs to visualize blood flow and used the phosphorescence decay method to measure oxygen tension. By exciting two dyes with two different wavelengths, both RBC velocity and oxygen tension could be measured continuously, but we had to ensure that the absorption and emission spectra of the fluorescence dye used for visualizing RBC flow and the phosphorescence dye used for measuring oxygen tension did not overlap. In addition, we had to determine how the measurement accuracy was affected by excitation light passing through the targeted microvessel and exciting the oxygen probe dye in the brain tissue beneath it.

The aim of this study was to develop a fluorescence and phosphorescence system that can simultaneously measure the cerebral microcirculatory distribution and the oxygen tension in cerebral microvessels. We examined the emission and absorption spectra of fluorescence and phosphorescence dyes, the spatial resolution, the half-life of probe dye in blood, the extravasation of the dye, and the phosphorescence emission from the tissue lying under the targeted microvessels. To demonstrate the feasibility of our system, we performed animal experiments involving acute hemorrhagic shock.

Address for reprint requests and other correspondence: K. Tsukada, Dept. of Physiology, Kawasaki Medical School, 577 Matsushima, Kurashiki, Okayama 701-0192 Japan (E-mail: ktsukada@med.kawasaki-m.ac.jp).

The costs of publication of this article were defrayed in part by the payment of page charges. The article must therefore be hereby marked "*advertisement*" in accordance with 18 U.S.C. Section 1734 solely to indicate this fact.

MATERIALS AND METHODS

Animal preparations. All animals received humane care in compliance with the "Guide for the Care and Use of Laboratory Animals" prepared by the Animal Research Committee of the Kawasaki Medical School. Male Wistar rats weighing 300–350 g were anesthetized with an intraperitoneal injection of α-chloralose (60 mg/kg) and urethane (600 mg/kg). The head of each rat was fixed in a stereotaxic frame, and the left parietal bone was exposed by a longitudinal midline skin incision. After three polyethylene tubes (PE-50) were fixed to the skull with cyanoacrylate, a craniectomy was performed, and a closed cranial window (5 mm in diameter) was made using a cover glass and a rubber O-ring. Artificial cerebrospinal fluid consisting of 147.8 meq/l Na^+, 3.0 meq/l K^+, 2.3 meq/l Mg^{2+}, 2.3 meq/l Ca^{2+}, 135.2 meq/l Cl^-, 19.6 meq/l HCO_3^-, 1.7 meq/l lactate, 1.1 mM phosphate, and 3.9 mM glucose was superfused at 0.1 ml/min. A thermistor with a diameter of 2.3 mm was fitted to the cranial window to monitor the temperature, and the cerebral fluid was maintained at 37°C. The left femoral artery was cannulated for monitoring the mean arterial blood pressure (MAP), the right femoral artery was cannulated for withdrawing blood, and the right femoral vein was cannulated for infusing blood or drugs.

Probe administration for RBC flow visualization and oxygen measurement. The RBC flow in cerebral microvessels was visualized by perfusing RBCs labeled with fluorescent isothiocyanate (FITC, Sigma Chemical) as described by Ishikawa et al. (3). Blood was withdrawn from the donor rat, and the RBCs were centrifuged and washed. The FITC was excited by irradiating it at an energy density of 5 mW/cm^2 with the light from a mercury lamp and passing it through a band-pass filter (450–490 nm). Each rat received 0.1 ml of FITC-labeled RBC suspension injected into its cannulated femoral vein. (This amount of FITC-labeled RBCs accounted for ~1/50 of all the RBCs in the body.)

Image processing of fluorescent blood flow. Figure 1 shows a block diagram of the system used for measuring RBC velocity, vessel diameter, and oxygen tension in individual microvessels of the cerebral cortex. Microscopic images made with the FITC-emitted light that had passed through a long-pass filter (>520 nm) were recorded with a charge-coupled device camera equipped with an image intensifier (C6653MOD, Hamamatsu Photonics). The images were processed automatically by using a previously developed system (21). Briefly, this system consists of a host computer, a Hi8 video recorder, and an image-data-processing board. One frame of a still image can be viewed on the monitor via the image-processing board, which takes two still 512 × 512-pixel images, and the intensity can be digitized to 256 levels. Automated velocity measurement was made possible by writing C-language sequences to load the images into memory, calculate the correlation, fast-forward through the video frames, and so on.

Oxygen tension measurement using phosphorescence decay. The Pd-meso-tetra-(4-carboxyphenyl)-porphyrin (Pd-TCPP, Porphyrin Products) used as the phosphorescent probe for the O_2-dependent quenching was dissolved (20 mg/ml) in physiological saline containing bovine serum albumin and buffered to a pH of 7.4 with phosphate buffer. Each rat received a bolus of Pd-TCPP (30 mg/kg) through a slow intravenous injection, and the Pd-TCPP in the microvessels was excited by using the second harmonic of a Q-switched Nd:YAG pulse laser (532-nm wavelength, 6-ns pulse width at half maximum, 1-Hz pulse recurrence frequency, 200-nJ/pulse irradiation energy) through the objective lens of a microscope. Phosphorescence passing through a long-pass filter (>620 nm) was detected with a photomultiplier tube (PMT) (R1894, Hamamatsu Photonics). The voltage signal (current signal converted with resistance of 50 kΩ) from the PMT was fed into a personal computer via an analog-to-digital converter (NR-2000, Keyence) with a sampling frequency of 200 kHz and a sampling number of 500 points. When the decay signal was processed for use in calculating the phosphorescence lifetime, the first 10 sampling points (corresponding to 50 μs) from the start of sampling were excluded because they included the intensity of the exciting laser

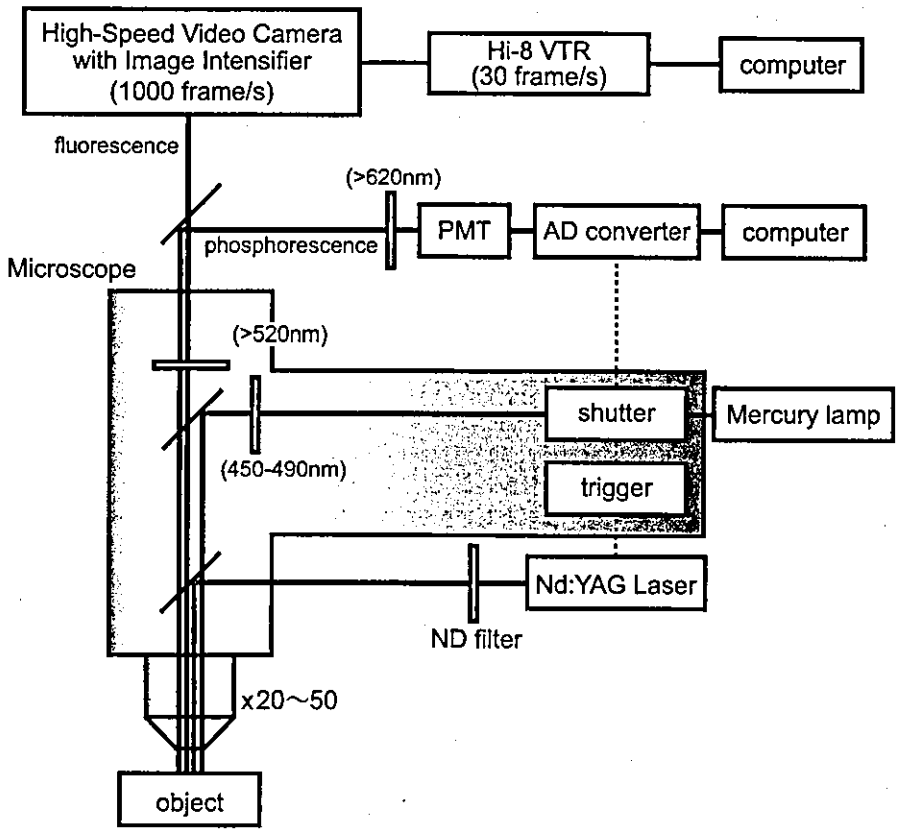

Fig. 1. Block diagram of system used for measuring red blood cell (RBC) flow velocity and oxygen tension in cerebral microvessels. To irradiate FITC for visualizing flow distribution and Pd-meso-tetra-(4-carboxyphenyl)-porphyrin (Pd-PCPP) for measuring oxygen tension alternately, a mechanical shutter was used to control the output of a mercury lamp and the signal from a limit switch was used to trigger an Nd:YAG laser when the shutter was closed. Blood flow images recorded with a charge-coupled device camera were used to automatically measure flow velocity by computer. PMT, photomultiplier tube; VTR, video tape recorder; AD, analog to digital; ND, neutral density.

light, which was not completely blocked by the long-pass filter. In addition, <1% of the maximum intensity of the PMT signal was rejected to reduce the contribution of dark current generated by the PMT. Phosphorescence lifetime τ was obtained by least-squares fitting of the remaining data to a single exponential curve. The oxygen tension (P_{O_2}) was calculated from the Stern-Volmer equation

$$I_0/I = \tau_0/\tau = 1 + k_q \cdot \tau_0 \cdot P_{O_2} \quad (1)$$

where I_0 and τ_0 are phosphorescence intensity and lifetime in the absence of oxygen, I and τ are the intensity and lifetime at a given oxygen tension, and k_q is the rate constant of oxygen quenching. The k_q and τ_0 values for our system were obtained from a calibration experiment using oxygen electrodes; at 37°C with a pH of 7.4 they were 374 $Torr^{-1} \cdot s^{-1}$ and 0.74 ms.

Irradiation timing of two light sources. To obtain two physiological values, the cerebral microcirculatory blood flow distribution and oxygen tension, we had to alternately irradiate each of two dyes in a targeted microvessel with the light from two excitation light sources. To measure the RBC velocity and oxygen tension at 1 Hz, we used a mechanical shutter to control the output of a mercury lamp and used the signal from a limit switch to trigger an Nd:YAG laser when the shutter was closed. The irradiation times of the laser and mercury lamp were, respectively, 6 ns and 300 ms.

Estimation of Pd-TCPP concentration in blood plasma. After five rats received 30 mg/kg of Pd-TCPP in solution (20 mg/ml) by slow injection into the femoral vein, blood samples were removed from the postcaval vein with a heparinized syringe at 5 and 30 min and at 1, 3, and 6 h. The plasma was extracted by centrifuging the samples at 1,500 rpm for 15 min; the skimming fluid taken as a measurement sample was obtained by additional centrifugation at 1,000 rpm for 5 min. The Pd-TCPP concentration in the plasma sample was quantified by absorption spectrophotometry, using the relation between absorbance and concentration previously calibrated at Pd-TCPP concentrations of 0.50, 0.25, 0.13, and 0.06 mg/ml (data not shown).

Narrow capillary model. Because the spatial resolution depends on the diameter of the laser spot, the effect of the spot size on lifetime was determined by changing the objective lens of the microscope. A narrow glass capillary with a 410-μm outer diameter and a 350-μm inner diameter was used as a microvessel model; it was set in a cranial window made by using the same materials and conditions as for the in vivo experiments. A solution of Pd-TCPP deoxygenized with sodium sulfite was kept at 37°C and a pH of 7.4 and perfused through the glass capillary. The phosphorescence intensity and lifetime were measured at different resolutions (i.e., spot sizes) by changing the magnification of the objective lens (×20 or ×50).

Flushing blood from microvessels. To photoexcite Pd-TCPP defused into extravascular cerebral tissue (i.e., not in microvessels), we inserted a catheter tube 0.8 mm in diameter into the left common carotid artery in the direction of the middle cerebral artery, and we fixed the edge of the tube at the internal carotid artery. After preparing the closed cranial window on the left parietal bone and administering the Pd-TCPP, we left the rat for 1 h so that the Pd-TCPP had sufficient time to leak from the microvessels into the extravascular tissue. Then, while applying continuous laser irradiation to a venule, we gave the rat an overdose of pentobarbital sodium, reducing both the MAP and heart rate to 0. Physiological saline was immediately infused via a carotid artery, flushing the blood and Pd-TCPP from the microvessels, and the targeted microvessel was observed with a microscope to verify that it was filled with saline. The phosphorescence emission from the Pd-TCPP that had leaked into the tissue was measured at a constant laser power before and after the flush.

Acute hemorrhagic shock model. Four rats were put into acute hemorrhagic shock by letting them bleed from a catheter in the femoral artery. They were bled, at 7–8 ml/min, to a MAP of 40 mmHg in <1 min. The shed blood was collected in heparinized syringes and kept at 37°C. The MAP was maintained at 40 ± 3 mmHg for 5 min by intermittently withdrawing 0.3–0.4 ml of blood. After the period of shock, the rats were resuscitated by infusing autologous whole blood.

RESULTS

Absorption and emission spectrum of FITC and Pd-TCPP. The absorption and emission spectra of the FITC used for labeling the RBCs and Pd-TCPP used as the oxygen-sensitive probe are shown in Fig. 2. For RBC velocity and oxygen tension to be measured simultaneously, the Pd-TCPP absorption must be extremely small in the wavelength band used to excite the FITC (from 460 to 490 nm). The Q-band of the Pd-TCPP was observed near 532 nm, which is the wavelength of the second harmonic of the Nd:YAG laser.

Simultaneous measurement of RBC velocity and oxygen tension. Figure 3*A* shows the microcirculatory vessel structure in the cerebral cortex observed in the closed cranial window. Figure 3*B* shows a high-magnification blood flow image with FITC-labeled RBCs. Figure 3*C* shows an image of laser light irradiating a targeted microvessel to measure the oxygen tension in the vessel. The RBC velocity and oxygen tension were

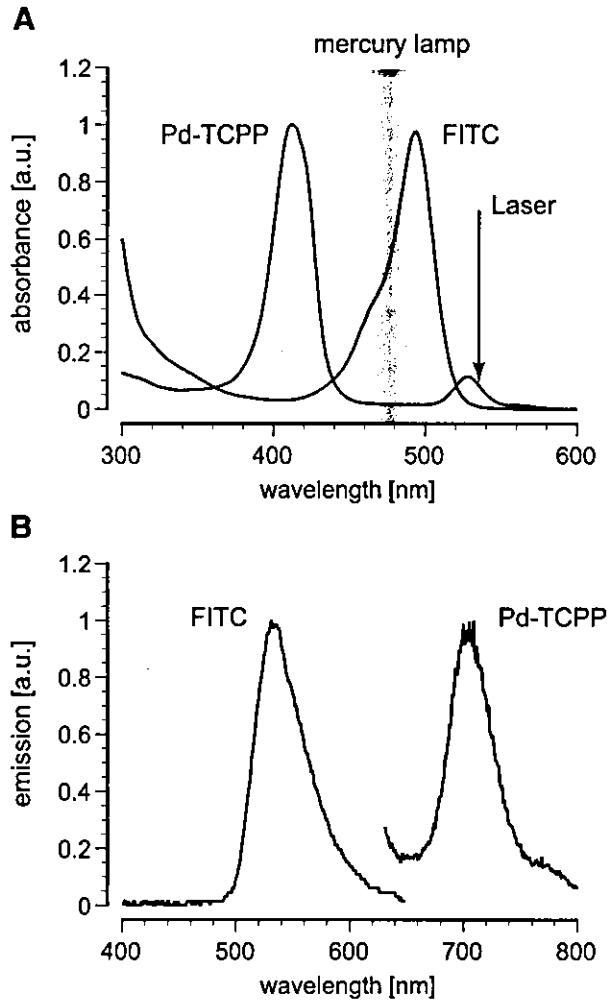

Fig. 2. Absorption (*A*) and emission (*B*) spectra of FITC used for labeling RBCs and Pd-TCPP used as oxygen-sensitive probes. Pd-TCPP absorption was extremely small in the band exciting the FITC (from 460 to 490 nm), and FITC absorption was small at the 532-nm wavelength exciting the Pd-TCPP. a.u., Arbitrary units.

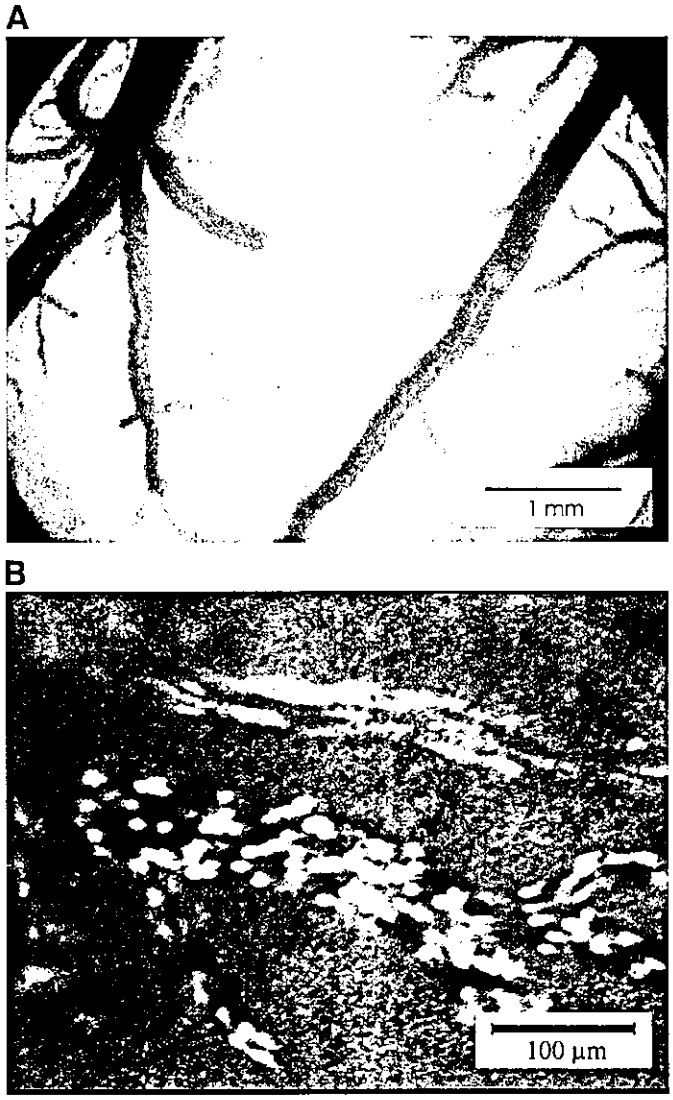

Fig. 3. Microscopic images of cerebral microvessel structure observed in closed cranial window (*A*), high-magnification blood flow of cerebral microcirculation visualized with FITC-labeled RBCs (estimated to be ~2% of all circulating RBCs) (*B*), and image of laser light irradiating a targeted microvessel to measure oxygen tension (*C*). Irradiation times of mercury lamp in *B* and laser in *C* were, respectively, 300 ms and 6 ns.

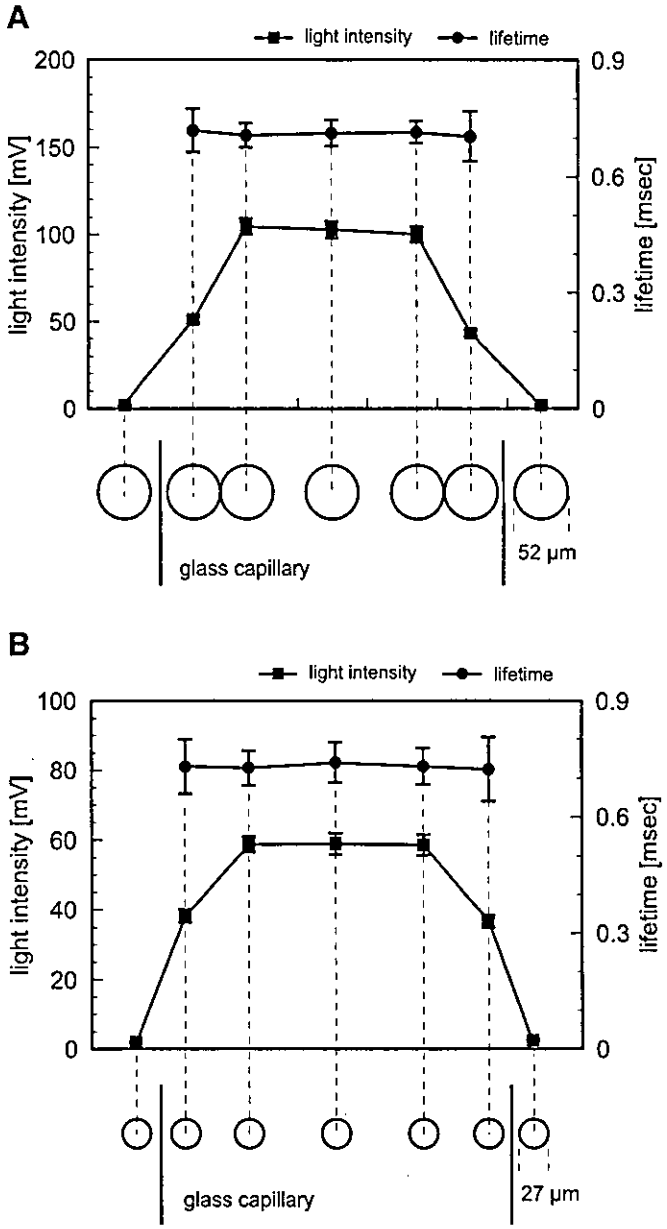

Fig. 4. Effect of laser spot size on measurement accuracy was small. Laser spot diameter, 52 (*A*) and 27 μm (*B*), i.e., the spatial resolution, was determined by magnification of objective lens: ×20 (*A*) and ×50 (*B*). A narrow glass capillary tube with a 410-μm outer diameter and a 350-μm inner diameter was filled with Pd-TCPP solution and used as a microvessel model. Even when the phosphorescence intensity was lower for spots near the wall, the lifetime was not affected at either resolution, indicating that stable oxygen measurement can be obtained by irradiating the inside of the microvessel. Values are means ± SD for 20 laser irradiations.

measured alternately at 1 Hz by using the shutter installed in the microscope to change between the two light sources (Nd:YAG laser and mercury lamp). After a microvessel was chosen for measurement, the microscope stage was positioned so as to direct the laser into the targeted vessel.

Spatial resolution. The phosphorescence intensity and lifetime at various locations in a glass capillary under different laser spots are shown in Fig. 4, *A* and *B*. Values are expressed as means ± SD for 20 laser irradiations. The phosphorescence lifetimes at the center were 0.72 ± 0.03 and 0.74 ± 0.05 ms

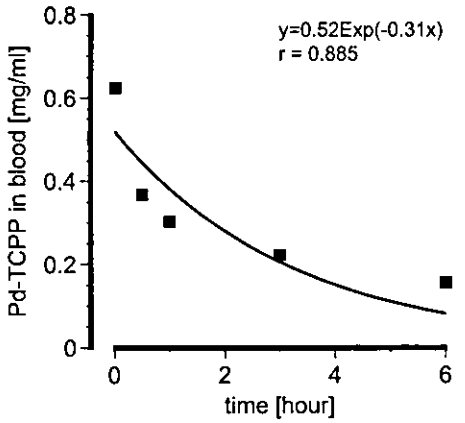

Fig. 5. Blood concentration curve obtained after bolus injection of Pd-TCPP. Leakage of Pd-TCPP from microvessels to extravascular tissue was observed. Fitting this data to an exponential decay curve yielded the equation $y = 0.52 \exp(-0.31x)$, $r = 0.885$, and 2.23 h for the half-life of Pd-TCPP in blood.

with ×20 and ×50 magnification, which was almost equivalent to τ_0. The laser spot, as measured from the irradiated images, was ~52 and 27 μm in diameter with objective lenses with ×20 and ×50 magnification, respectively. The phosphorescence lifetime remained about the same, even though the intensity decreased as the spot approached the wall because the amount of irradiated Pd-TCPP near the capillary wall was less than at the center in the Z-axial direction.

Pd-TCPP half-life in blood. Figure 5 shows the blood concentration after bolus injection of Pd-TCPP. Five minutes after the injection, the plasma concentration of Pd-TCPP was 624.7 μg/ml. At 0.5, 1, 3, and 6 h, the concentrations were, respectively, 366.2, 302.5, 222.2, and 155.7 μg/ml. Fitting this data to an exponential decay curve yielded 2.23 h for the half-life of Pd-TCPP in blood.

Phosphorescence emission from cerebral tissue after flushing blood from microvessels. Figure 6, *A* and *B*, shows, respectively, the decay curves of the phosphorescence before and after flushing the blood from the microvessels, and Fig. 6, *C* and *D*, shows, respectively, the log-intensity plots of the data in *A* and *B*. After the subject rat was killed, the oxygen tension calculated from the phosphorescence decay curves, obtained both before and after flushing, was 0.9 Torr. Correlation coefficient r^2 for the data in the valid area could be fitted to a single exponential function (0.998), suggesting that phosphorescence decay can be detected with high sensitivity and that lifetime can be calculated with high accuracy. In contrast, the phosphorescence intensity from the microvessel from which Pd-TCPP had been flushed with physiological saline was

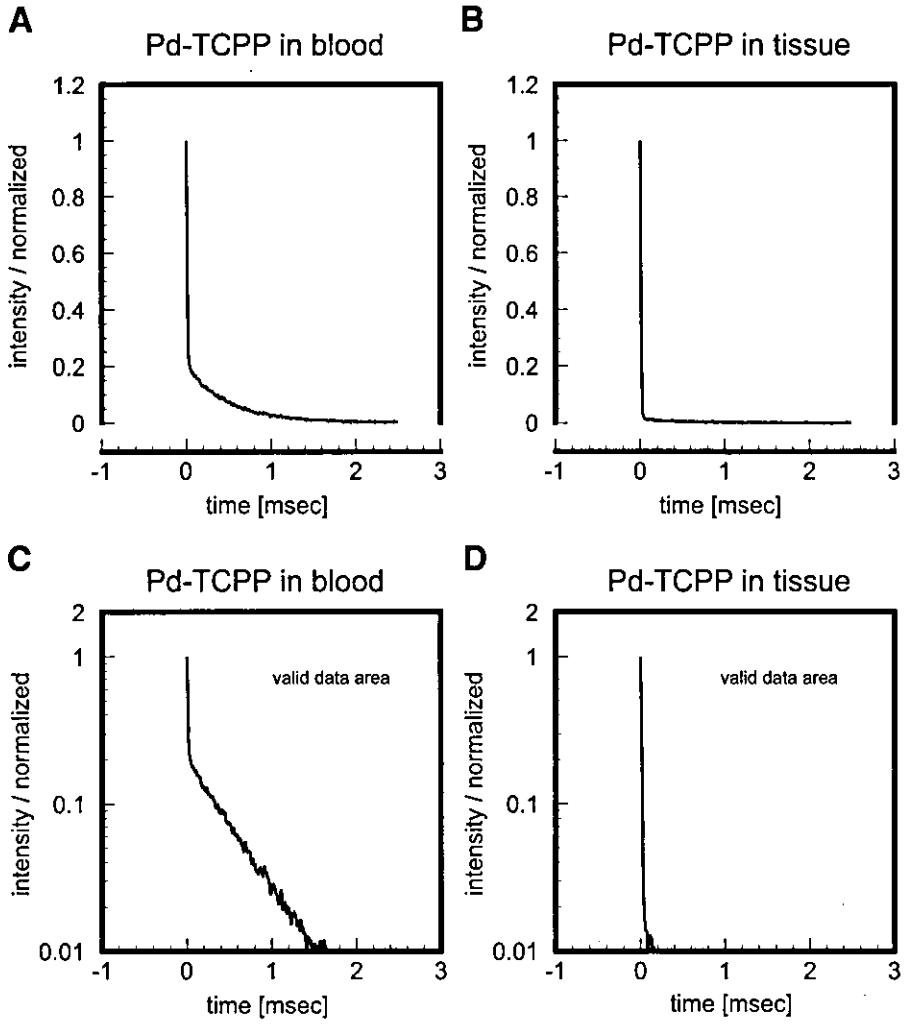

Fig. 6. Phosphorescence emission from Pd-TCPP in tissue was estimated by irradiating microvessels with a laser beam after flushing the blood from them. *A* and *B*: decay curves of phosphorescence before and after flushing. *C* and *D*: log-intensity plots of the data shown in *A* and *B*. Decay signals used for calculating oxygen tension were taken from "valid data areas" in *C* and *D*.

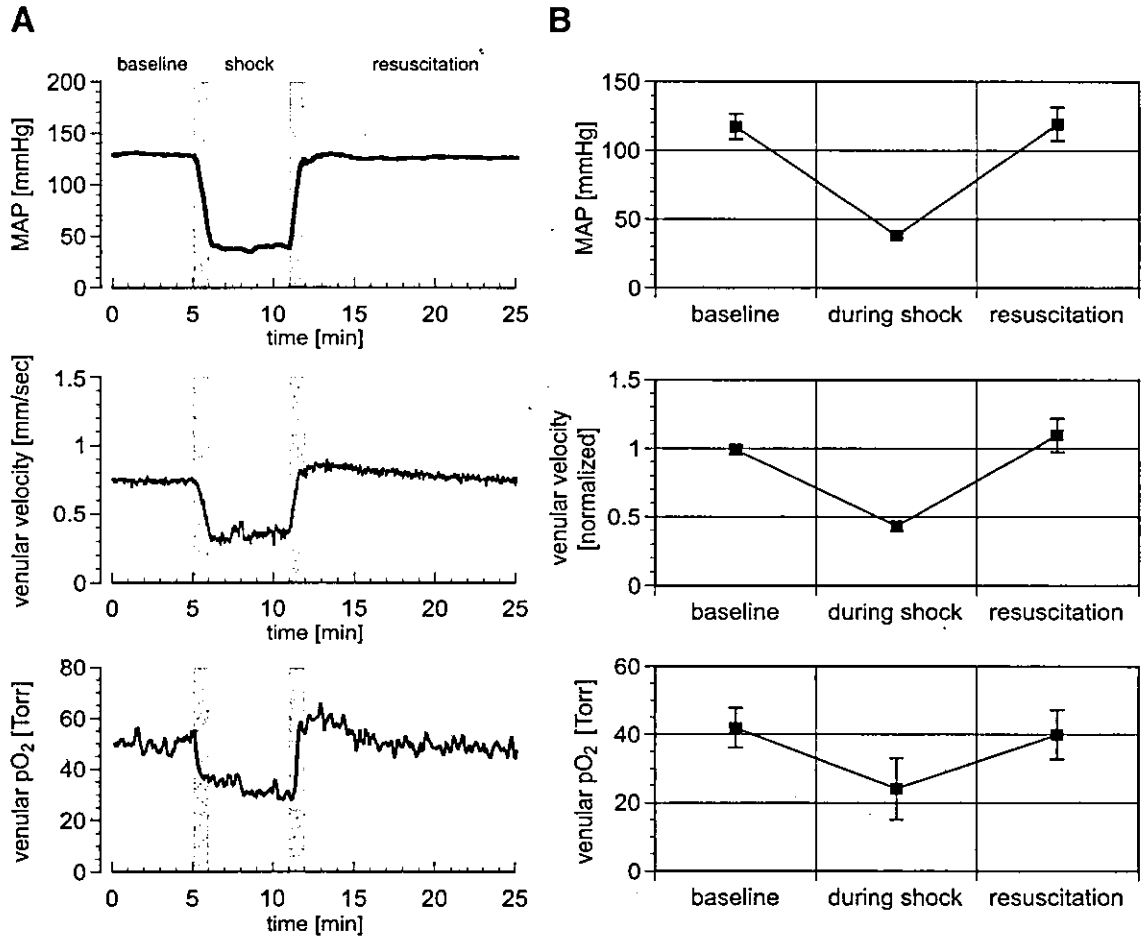

Fig. 7. Typical changes in mean arterial blood pressure (MAP), RBC velocity, and oxygen tension in venules during acute hemorrhagic shock. Blood was bled from a catheter in the femoral artery until the arterial pressure reached a mean of 40 mmHg; after the rats entered a period of shock, they were resuscitated by infusing autologous whole blood. Gray bars in *A* indicate the periods of bleeding and infusing blood. The average ± SD values of these variables (n = 4) before bleeding (baseline), during shock, and for 10 min after resuscitation are shown in *B*.

greatly reduced. As described above, the valid data for calculating the phosphorescence lifetime are the data gathered starting 50 μs after data acquisition. The greatest phosphorescence intensity (voltage signal from PMT) in this range was 15.4 mV in blood (Fig. 6*A*) and 1.9 mV in tissue (Fig. 6*B*). And shown in Fig. 6*D*, the sampling signal in the valid data area was extremely low, suggesting that there was very little phosphorescence emission from the extravascular tissue.

Hemorrhagic shock and resuscitation. Typical changes in the MAP, RBC velocity, and oxygen tension in the venules are shown in Fig. 7*A*, where we can see that the changes in the venular velocity and oxygen tension were synchronized to the change in MAP. The average values of these variables (n = 4) before bleeding (baseline), during shock, and for 10 min after resuscitation are shown in Fig. 7*B*. MAP fell from 117.3 ± 9.2 to 38.2 ± 1.4 mmHg during shock and then increased to 119.3 ± 11.9 mmHg after resuscitation. The venular velocity dropped to 43 ± 4% of its baseline value and then increased to 110 ± 12% of its baseline value. The venular oxygen tension fell from 41.9 ± 5.8 to 24.0 ± 9.0 Torr and then increased to 40.0 ± 7.2 Torr.

DISCUSSION

We set up and evaluated the effectiveness of our optical system for measuring the RBC velocity and oxygen tension in cerebral microcirculation simultaneously and continuously by using the difference in wavelength and luminescence between fluorescence and phosphorescence. We also examined factors affecting the accuracy of our phosphorescence photometry measurements through in vitro experiments.

Simultaneous measurement of RBC velocity and oxygen tension. Because brain cells store hardly any oxygen or substrates, brain function depends on microcirculation. An extremely efficient way to analyze cerebral microcirculatory regulation would thus be to simultaneously measure the RBC velocity and oxygen concentration in microregions. However, there is no convenient equipment suitable for measuring these two parameters continuously and simultaneously. Liss and Liss (8) monitored tissue oxygen pressure in flap microcirculation with electrodes and measured blood flow velocity by using the laser-Doppler method. In macroscopic measurement of tissue oxygenation, these techniques are probably easy to use. With regard to measurement in microcirculation, Parthasarathi and

Lipowsky (9) used oxygen electrodes to measure the oxygen in rat cremaster muscle and used the two-slit technique to measure blood flow in the muscle. Although oxygen electrodes can be used to measure the oxygen tension in various types of tissue, they cannot be used in blood vessels (especially microvessels) because their use requires physical invasion. The phosphorescence decay method using the photochemical reaction between porphyrin dye and oxygen molecules makes it possible to measure oxygen tension noninvasively, to obtain the local oxygen concentration with high spatial resolution, and to obtain the absolute partial pressure instead of a relative value.

Systems based on phosphorescence decay can be roughly divided into two types: those that can be used to draw oxygen mappings and those that can provide one-point measurements suitable for microcirculation study. The former type has been applied to kidney (11), liver (25), the carotid body (7), cells (10), and brain (24) and has also been used in ophthalmology (16) and in cancer studies (23). Shonat et al. (15) imaged hemoglobin saturation and oxygen tension in the cerebral cortex of mice. The latter type can be used to measure the local oxygen tension in tissue or in microvessels by focusing excitation light through the objective lens of a microscope (1, 2, 6, 13, 18). Kerger, Tsai, and colleagues (5, 19, 20) applied it and used the photodiode correlation method to measure blood velocity in dorsal skin microcirculation while using originally developed equipment to measure the diameter of the microvessels. As explained in the introduction, however, when researchers needed to measure both RBC velocity and oxygen tension, they were restricted to two-dimensional tissue samples.

As shown in Fig. 7, both venular velocity and oxygen tension in microvessels were synchronized to changes in blood pressure. The phosphorescence decay method has been used to evaluate the physiological reactions in certain organs during hemorrhagic shock (4, 14). Song et al. (17) reported deterioration in the oxygen tension in cortical tissue caused by hemorrhagic hypotension and recovery with PEG solution in piglet brain, and Yonetani et al. (26) reported a decrease in the cortical oxygen pressure with decreasing arterial pressure. However, quantified oxygen fluctuation with changes in the microcirculatory distribution in the cerebral cortex has not been reported.

Measurement accuracy and spatial and time resolution. As shown in Fig. 4, the phosphorescence lifetime was stable at each resolution when the laser spot was inside the targeted microvessel, even when the phosphorescence intensity decreased. This indicates that measurements should be stable if the phosphorescence lifetime is stable, even if the phosphorescence intensity decreases because of a decrease in Pd-TCPP in the blood. Also, as shown in Fig. 4, the spatial resolution increased when the magnification was increased, meaning that the measurement of the true capillaries is theoretically possible (27). However, increasing the magnification reduces the volume of phosphorescent light received, and, in the case of true capillaries, the volume of Pd-TCPP in the vessels also decreases, so measurement accuracy drops noticeably, meaning that the noise and the error rate will increase.

The time resolution of our measurements was 1 s because the laser irradiation frequency was set at 1 Hz (although the maximum was 110 Hz). Increasing the irradiation frequency and adding the decay curves to smooth them reduces the noise in the phosphorescence signals. However, as shown in Fig. 6, clear decay curves with little noise were obtained by one-shot irradiation, indicating that 200 nJ of pulse energy is sufficient for measurement. Moreover, increasing the pulse irradiation would create excessive singlet oxygen production. Measurement in milliseconds is more than sufficient for a vital reaction. For these reasons, a time resolution of 1 s is sufficient for continuous measurement of oxygen tension.

Reactive oxygen caused by double-wavelength photoexcitation. We monitored RBC velocity and oxygen tension in rat brain microcirculation simultaneously by injecting RBCs labeled with FITC and oxygen probe Pd-TCPP and then exciting these probe dyes by irradiation from a mercury lamp and an Nd:YAG laser, respectively. Exciting photosensitive substances like porphyrin dyes inevitably generates reactive oxygen in microvessels, and reactive oxygen, especially singlet oxygen, causes thrombus formation, which can affect blood flow. We tested continual irradiation of capillaries in intestinum tenue for 10 min but did not observe any change in flow velocity (data not shown). This result depends on not much light energy being needed to measure phosphorescence and the irradiation time being extremely short. In contrast, the excitation light for visualizing the FITC-labeled RBCs came from a mercury lamp and passed through a band-pass filter (450–490 nm) while the shutter was open. The stronger the excitation light, the sharper the images we can create for measuring RBC velocity. When the microvessels were irradiated with high power, however, flow stasis in the vessels was observed within a few minutes. Singlet oxygen must be suppressed to reduce thrombus formation and stasis as much as possible, so we decreased the irradiation power to <5 mW/cm^2 and equipped the recording camera with an image intensifier. We observed no stasis and obtained clear blood flow images.

Phosphorescence emission from tissue under microvessels. When the oxygen tension in a single microvessel in the cerebral cortex is measured, the laser light irradiated through the microscope's objective lens should pass through the microvessel. The measured value may thus be affected by the excitation of Pd-TCPP in the tissue under the targeted microvessel. The oxygen concentration in brain tissue is considerably lower than that of blood in a microvessel, so any mixing of the phosphorescence emitted from intravascular Pd-TCPP with that emitted from interstitial Pd-TCPP would artifactually reduce the measured oxygen concentration in a blood vessel. The effect of this mixing on the measured concentration needs to be investigated. Moreover, the effects of a laser light irradiated not from a confocal system but from a conventional incident-light system also need to be investigated. The main reason that the phosphorescence from the tissue irradiated though a microvessel was extremely weak is attributed to the focusing of the laser light by the objective lens. The irradiation angle of laser light depends on the numerical aperture. The microvessel was irradiated at an angle, not vertically, and the profile of the laser intensity was Gaussian. Consequently, the excitation energy is thought to have been focused in the laser spot area and at the focal depth of the objective lens. For instance, at a wavelength of 532 nm, the focal depth of the objective lens we used, which had a numerical aperture of 0.4, is theoretically 1.7 μm. Therefore, even when scattering by blood is taken into consideration, when the light was focused in a microvessel almost 50 μm in diameter, little excitation light

could have reached the underlying extravascular tissue by passing through the vessel.

In summary, we measured the RBC velocity and oxygen tension in cerebral microcirculation by using the differences in luminescence and wavelength between fluorescence and phosphorescence. With this system, we can acquire information about cerebral microcirculatory distribution and oxygen tension simultaneously and easily. We evaluated our method by examining the factors causing measurement error. Because blood flow and oxygen concentration are associated in organs using large amounts of oxygen, particularly the brain, the heart, and the kidney, simultaneous measurement of the microcirculatory red cell velocity and local oxygen tension should be widely applicable to research.

ACKNOWLEDGMENTS

We thank Mami Ishikawa (Department of Neurosurgery, Keio University School of Medicine, Japan), for assisting with the experiments.

GRANTS

This research was partially supported by a Grant-in-Aid for Young Scientists (B) (15700340, 2003) from the Ministry of Education, Science, Sports and Culture and Kawasaki Medical School Research Project Grant 14-304 and 15-301A.

REFERENCES

1. **Buerk DG, Tsai AG, Intaglietta M, and Johnson PC.** In vivo tissue pO2 measurements in hamster skinfold by recessed pO2 microelectrodes and phosphorescence quenching are in agreement. *Microcirculation* 5: 219–225, 1998.
2. **Erni D, Sakai H, Tsai AG, Banic A, Sigurdsson GH, and Intaglietta M.** Haemodynamics and oxygen tension in the microcirculation of ischaemic skin flaps after neural blockade and haemodilution. *Br J Plast Surg* 52: 565–572, 1999.
3. **Ishikawa M, Sekizuka E, Shimizu K, Yamaguchi N, and Kawase T.** Measurement of RBC velocities in the rat pial arteries with an image-intensified high-speed video camera system. *Microvasc Res* 56: 166–172, 1998.
4. **Ince C and Sinaasappel M.** Microcirculatory oxygenation and shunting in sepsis and shock. *Crit Care Med* 27: 1369–1377, 1999.
5. **Kerger H, Saltzman DJ, Gonzales A, Tsai AG, van Ackern K, Winslow RM, and Intaglietta M.** Microvascular oxygen delivery and interstitial oxygenation during sodium pentobarbital anesthesia. *Anesthesiology* 86: 372–386, 1997.
6. **Kerger H, Torres Filho IP, Rivas M, Winslow RM, and Intaglietta M.** Systemic and subcutaneous microvascular oxygen tension in conscious Syrian golden hamsters. *Am J Physiol Heart Circ Physiol* 268: H802–H810, 1995.
7. **Lahiri S, Rumsey WL, Wilson DF, and Iturriaga R.** Contribution of in vivo microvascular P_{O_2} in the cat carotid body chemotransduction. *J Appl Physiol* 75: 1035–1043, 1993.
8. **Liss AG and Liss P.** Use of a modified oxygen microelectrode and laser-Doppler flowmetry to monitor changes in oxygen tension and microcirculation in a flap. *Plast Reconstr Surg* 105: 2072–2078, 2000.
9. **Parthasarathi K and Lipowsky HH.** Capillary recruitment in response to tissue hypoxia and its dependence on red blood cell deformability. *Am J Physiol Heart Circ Physiol* 277: H2145–H2157, 1999.
10. **Robiolio M, Rumsey WL, and Wilson DF.** Oxygen diffusion and mitochondrial respiration in neuroblastoma cells. *Am J Physiol Cell Physiol* 256: C1207–C1213, 1989.
11. **Rumsey WL, Abbott B, Lo LW, Vinogradov SA, and Wilson DF.** Imaging of oxygen distribution in the surface and deep areas of the kidney. *Adv Exp Med Biol* 411: 591–595, 1997.
12. **Rumsey WL, Vanderkooi JM, and Wilson DF.** Imaging of phosphorescence: a novel method for measuring oxygen distribution in perfused tissue. *Science* 241: 1649–1651, 1988.
13. **Sinaasappel M and Ince C.** Calibration of Pd-porphyrin phosphorescence for oxygen concentration measurements in vivo. *J Appl Physiol* 81: 2297–2303, 1996.
14. **Sinaasappel M, van Iterson M, and Ince C.** Microvascular oxygen pressure in the pig intestine during haemorrhagic shock and resuscitation. *J Physiol* 514: 245–253, 1999.
15. **Shonat RD, Wachman ES, Niu W, Koretsky AP, and Farkas DL.** Near-simultaneous hemoglobin saturation and oxygen tension maps in mouse brain using an AOTF microscope. *Biophys J* 73: 1223–1231, 1997.
16. **Shonat RD, Wilson DF, Riva CE, and Cranstoun SD.** Effect of acute increases in intraocular pressure on intravascular optic nerve head oxygen tension in cats. *Invest Ophthalmol Vis Sci* 33: 3174–3180, 1992.
17. **Song D, Olano M, Wilson DF, Pastuszko A, Tammela O, Nho K, and Shorr RG.** Comparison of the efficacy of blood and PEG-hemoglobin in recovery of newborn piglets from hemorrhagic hypotension. *Transfusion* 35: 552–558, 1995.
18. **Torres Filho IP and Intaglietta M.** Microvessel P_{O_2} measurements by phosphorescence decay method. *Am J Physiol Heart Circ Physiol* 265: H1434–H1438, 1993.
19. **Torres Filho IP, Kerger H, and Intaglietta M.** P_{O_2} measurements in arteriolar networks. *Microvasc Res* 51: 202–212, 1996.
20. **Tsai AG, Friesenecker B, McCarthy M, Sakai H, and Intaglietta M.** Plasma viscosity regulates capillary perfusion during extreme hemodilution in hamster skinfold model. *Am J Physiol Heart Circ Physiol* 275: H2170–H2180, 1998.
21. **Tsukada K, Minamitani H, Sekizuka E, and Oshio C.** Image correlation method for measuring blood flow velocity in microcirculation: correlation 'window' simulation and in vivo image analysis. *Physiol Meas* 21: 459–471, 2000.
22. **Vanderkooi JM and Wilson DF.** A new method for measuring oxygen concentration in biological systems. *Adv Exp Med Biol* 200: 189–193, 1986.
23. **Wilson DF and Cerniglia GJ.** Localization of tumors and evaluation of their state of oxygenation by phosphorescence imaging. *Cancer Res* 52: 3988–3993, 1992.
24. **Wilson DF, Pastuszko A, DiGiacomo JE, Pawlowski M, Schneiderman R, and Delivoria-Papadopoulos M.** Effect of hyperventilation on oxygenation of the brain cortex of newborn piglets. *J Appl Physiol* 70: 2691–2696, 1991.
25. **Wilson DF, Rumsey WL, and Vanderkooi JM.** Oxygen distribution in isolated perfused liver observed by phosphorescence imaging. *Adv Exp Med Biol* 248: 109–15, 1989.
26. **Yonetani M, Huang CC, McGowan J, Lajevardi NS, Pastuszko A, Delivoria-Papadopoulos M, and Wilson DF.** Effect of hemorrhagic hypotension on extracellular level of dopamine, cortical oxygen pressure and blood flow in brain of newborn piglets. *Neurosci Lett* 180: 247–252, 1994.
27. **Zheng L, Golub AS, and Pittman RN.** Determination of P_{O_2} and its heterogeneity in single capillaries. *Am J Physiol Heart Circ Physiol* 271: H365–H372, 1996.

3-S14-1

生命情報のセンシング
ー多波長励起フォトニックイメージングシステムによる機能解析ー

南谷晴之(慶応義塾大学)，塚田孝祐(川崎医科大学)，
関塚永一（国立埼玉病院），大塩　力（亮友会大塩医院）

Biosignal Sensing – A New Method for Cellular Function Analysis by Using Multi Photonic Imaging System –

Haruyuki Minamitani (Keio University), Kousuke Tsukada (Kawasaki Medical School),
Eiichi Sekizuka (National Saitama Hospital), Chikara Oshio (Oshio Clinic)

1．はじめに

蛍光･燐光発光分子、磁気微粒子、蛍光抗体などの物理的・生化学的作用に基づく分子認識機構を有する超極限分子プローブを用いて、生体内で起こる血管炎や微小循環障害によって誘発される種々の組織傷害や細胞傷害のメカニズムを分子・細胞レベルで解析・診断する超高感度イメージング技術を開発するとともに、その障害の発現メカニズムと障害からの再生・治癒過程に関する分子機序を局所的に解析し、診断治療への応用展開を目的として本研究を遂行した。その項目は、1)超極限分子を骨格とするナノ粒子プローブの開発と応用、2)高感度高速度バイオイメージング技術の開発と応用、3) 複数の異なるナノプローブの発光現象を利用する多波長励起マルチフォトニックイメージングシステムの開発と応用、4)組織細胞内の分子生理機能の時空間的計測・解析技術の開発と応用、5)糖尿病性細小血管障害・脳血栓など特異的な血流ダイナミクスのイメージング解析と薬理効果の評価、6)腫瘍新生血管の光化学反応に基づく血流遮断効果や糖尿病性微小循環における血管閉塞・血栓形成の解析と診断治療への応用である。

2．実験・解析方法

実質臓器や組織の微小循環レベルにおける血流動態や個々の血球細胞の挙動を可視化するには種々の蛍光標識プローブを利用するのが有効である。組織微小血管内の血行動態を可視化解析するために、FITC-dextran（励起波長488nm、蛍光波長 520nm）20mg/ml を iv 投与し、血漿成分の流動現象を可視化して、全血血流動態の定量化を行った。また、赤血球の流速を測定するために、予め、循環赤血球の約５％を採血し、これを体外で蛍光プローブ FITC（励起波長 488nm、蛍光波長 520nm）で ex-vivo 標識した後、返血し、顕微鏡下で微小血管を流れる個々の蛍光標識赤血球の流動現象を可視化した。白血球の可視化にはアクリジンオレンジ（励起波長 430nm、蛍光波長 530nm）0.5mg/kg を iv 投与し体内染色するか、ローダミン６G（励起波長 514nm、蛍光波長 590nm）50μg/ml で ex-vivo 標識して、微小血管内の白血球のローリングや粘着数を可視化計測した。一方、血小板の可視化には CFSE（励起波長 494nm、蛍光波長 520nm）かローダミン６G を iv 投与・体内染色するか、CFDASE で ex-vivo 標識して、微小血管内の流動、血小板血栓生成動態を可視化評価した。

これら血球細胞の挙動や血流動態の可視化解析には、高感度高速度CCDビデオイメージングシステム(Nippon Roper CR imge2000、浜松ホトニクスSIT）を、血球細胞の速度計測には画像相関法を用いて行った。FITC標識赤血球の流速計測と同時に光励起したPdポルフィリンからの燐光寿命より酸素分圧を計測する技術（蛍光・燐光ナノプローブを用いたフォトニック・イメージング解析法による臓器微小血管内の血流速度・酸素分圧同時計測法）を開発し利用した。予め、対象動物にPdポルフィリンをiv投与し、対象となる微小血管に励起パルス光（Nd：YAG laser SH、波長 532nm）を照射する。酸素濃度に依存して発光する燐光を 620nmのロングパスフィルタを介してフォトマルで光電変換し、AD変換後にパソコンで波形処理して、燐光寿命 τ より次のStern-Volmer式に基づいて酸素分圧 pO_2 を求めた。

$$\tau_0 / \tau = 1 + K \tau_0 pO_2$$

ここで τ_0、τ はそれぞれ酸素分圧が０および pO_2 mmHg のときの燐光寿命、KはStern-Volmer定数である。図１は多波長励起フォトニックイメージングシステムの概要を示す図である。これらの実験ではラットやマウスの*in-vivo*実験系でなされた。ラット・マウスを対象にした血栓形成モデルの構築にはポルフィリン系光感受性物質と特定波長励起光の相互作用に基づく光化学反応を利用し、活性酸素産生、

サイトカイン産生、酵素作用を解析した。

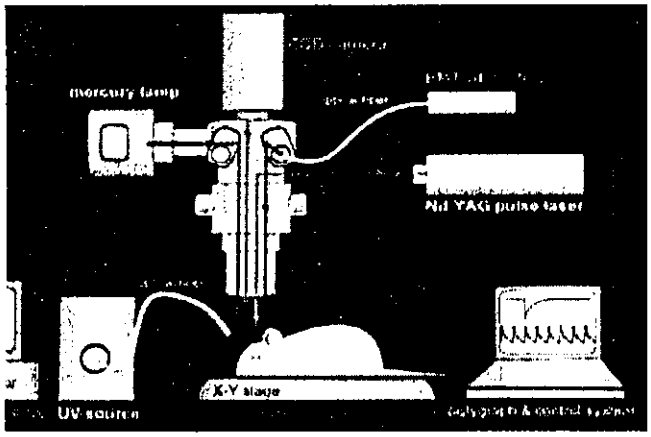

図1　多波長励起フォトニックイメージングシステム

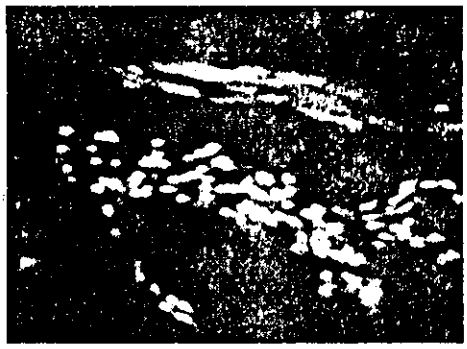

図2 FITC 標識赤血球による血流動態可視化

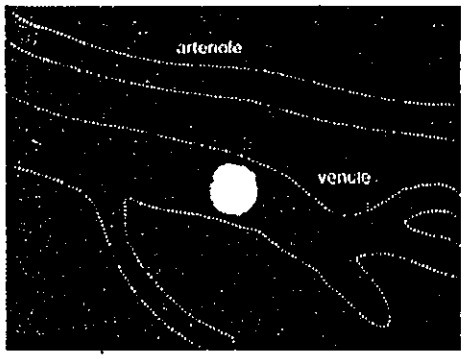

図3 レーザ照射による微小血管内酸素分圧計測

一方、血管障害や血栓形成に関わる血管内皮細胞(HUVEC)と血小板・白血球の相互作用を検討するために、培養細胞を用いた *in-vitro* 系において各種蛍光プローブを用いて細胞骨格形態の動的変化・細胞内分子機能変化の可視化解析および活性酸素種の同定と定量化を蛍光生体顕微鏡やリアルタイム共焦点走査型レーザ顕微鏡を用いて行った。また、Apoptosis を含む細胞機能や分子機能の分析にフローサイトメトリー、ウェスタンブロット法などの分析法も利用した。

3．実験・解析結果

微小循環障害・血栓形成に基づく血流停止・血管閉塞あるいは虚血応答をラットの腸間膜・肝臓・脳表層微小血管を対象に可視化解析した。図 2 は Wistar 系雄性ラットの closed cranial window 内で観測された脳表微小血管内の FITC 標識赤血球の流動状態を可視化したものである。また図3は同一血管中央部に Nd-YAG laser SH パルス光を照射したレーザスポットを示したものであり、この部位から酸素分圧に依存した燐光放射が観測される。この対象において脱血・返血による脳虚血・再潅流時の脳実質表層の血流動態と酸素代謝を定量化が可能となる。図 4 は血流速度と酸素分圧変化を示したもので、虚血状態で速度と酸素分圧の低下が観測され、短時間後の再潅流により元の状態に復帰することがわかる。

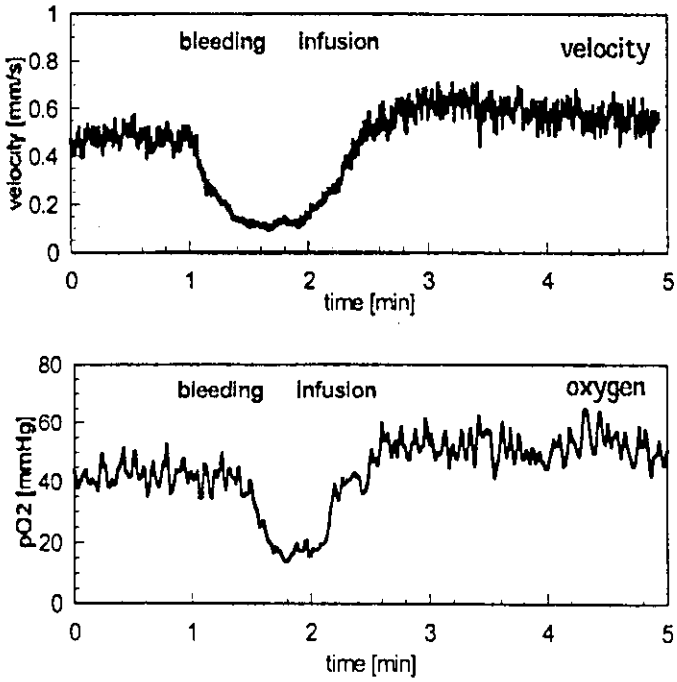

図4　急性虚血・再潅流における脳表層微小血管内の血流速度と酸素分圧変化

光化学反応は、光感受性物質の光励起によって産生される活性酸素が主体となって細胞傷害や血行障害を誘起させるものであり、apoptosis、necrosis の重要因子となるが、本研究では血小板血栓生成に関わる活性酸素の効果をラット腸間膜および脳表層微小血管で観測するとともに活性酸素種の同定を活性酸素消去剤のスカベンジャ作用によって評価した。図 5 はラット脳微小血管中の蛍光標識した血小板血栓形成過程の可視化イメージである。また、図 6 は腸間

模微小血管内の血栓形成過程における白血球のローリングと粘着状態を観測した可視化イメージである。

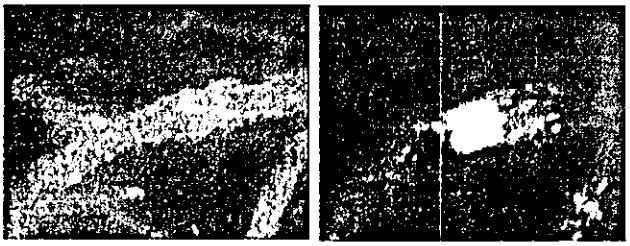

図5　蛍光標識血小板の微小血管内の血栓形成過程のイメージ

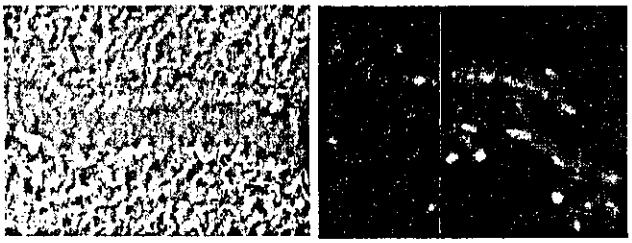

図6　蛍光標識白血球の微小血管壁へのローリングと粘着状態のイメージ

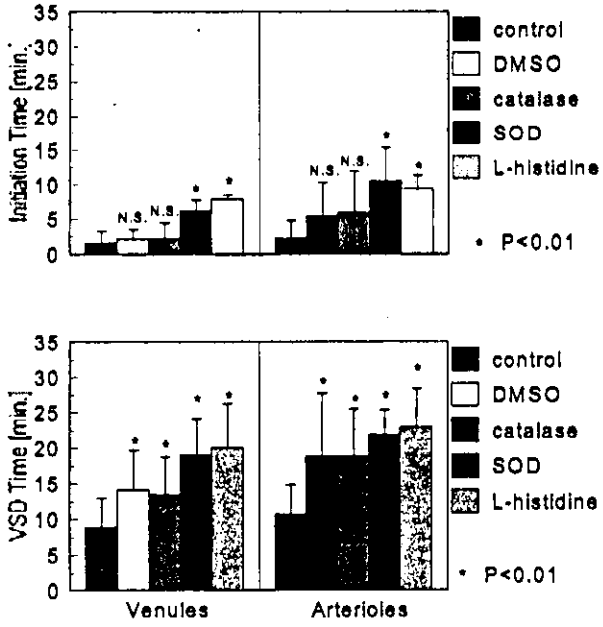

図7　微小血管内血栓形成過程における血小板粘着開始時間（initiation time）と完全血管閉塞・血流遮断時間（VSD time）ならびにスカベンジャによる活性酸素消去に基づく血小板粘着開始時間と血流遮断時間の延長

図7は微小血管の血栓形成過程における血小板粘着開始時間(initiation time)と完全血管閉塞・血流遮断時間（VSD time)ならびにスカベンジャによる活性酸素消去に基づく血小板粘着開始時間と血流遮断時間の延長を示した結果である。各活性酸素のスカベンジャは、一重項酸素$^1O_2$に対してLヒスチジン50mg/kg、スーパーオキシドアニオンO_2^-に対してSOD3mg/kg、過酸化水素H_2O_2に対してカタラーゼ3mg/kg、ヒドロキシラジカル・OHに対してDMSO1mg/kgを使用し、非適用群との相違を比較検討した。図7からわかるように活性酸素種のうち、一重項酸素とスーパーオキシドアニオンの関与が大であり、細動脈、細静脈ともに血小板粘着開始時間と血流遮断時間の有意な延長が認められた。このような血栓形成・血流遮断は、とくに糖尿病において顕著な速さで血小板粘着開始、血管閉塞が起こり、糖尿病における易血栓性が明らかとなった。この光化学反応による急性血栓モデルにおいて、赤血球速度、血小板粘着開始時間、血流遮断時間、接着白血球数などを計測し、健常状態と比較検討した結果、活性酸素産生に基づく活性化白血球・血小板及び内皮細胞の相互作用により内皮傷害、血小板膜破壊・脱顆粒・作用物質放出が促進され、カスケード的に血小板粘着能の亢進、凝固系の促進、血栓成長、血管閉塞に至る過程が確認された。糖尿病では赤血球の変形能の低下や赤血球膜の硬化が認められるので、血管内皮への傷害も増加するものと考えられる。また、腫瘍内微小血管の光化学反応による血流遮断効果を検討したところ、腫瘍血管内ではずり速度の低下、早期の血小板粘着開始と血流遮断が認められ、光化学治療における血流遮断効果の高さとその有効性が確かめられた。

一方、血管障害や血栓形成に関わる血管内皮細胞（HUVEC）と血小板・白血球の相互作用を検討するために、培養細胞を用いた*in-vitro*系において各種蛍光プローブを用いて細胞骨格形態の動的変化・細胞内分子機能変化の可視化解析をした。まず、Calcein-AM（励起300nm、蛍光510nm）染色した内皮細胞の形態変化を観測した結果、図8に見られるように、光化学反応の活性酸素産生により細胞短縮が起こり、内皮下基質の露出が顕著に増加することを確認した。このまま放置すると24時間後には元の形態に復する。

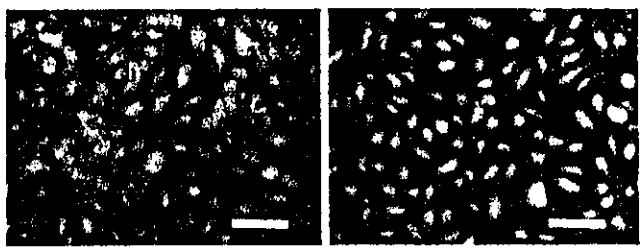

図8　Calcein-AM染色した内皮細胞の形態変化
（左）光化学反応前、(右)光化学反応後の活性酸素産生による細胞短縮と内皮下基質の露出が顕著に見られる。
Bar = 100 μm

また、図9に見られるように、Rhodamine-phalloidin（励

起 554nm、蛍光 573nm）で染色したアクチンフィラメントの可視化により、光化学反応後に球状タンパク質のGアクチンから線維状の細胞骨格Fアクチンへの重合が認められ、細胞の形態変化・短縮化・細胞先端部の増強に作用しているものと考えられた。図中、細胞中央部の明るく見える部分はDAPI（励起 358nm、蛍光 461nm）で染色した細胞の核を示している。図 10 は上記と同様に光化学反応の活性酸素産生による細胞接着を司っている tight junction の構成タンパク質 ZO-1 を免疫蛍光染色したイメージである。光化学反応前には細胞間に ZO-1 の線維状の確認されるが、光化学反応後にはタイトジャンクションの喪失、内皮下の露出が認められ、内皮細胞の短縮とともに細胞間間隙が広がり内皮下露出が顕著となる。細胞骨格Fアクチン重合及び tight junction の変化は、このまま放置すると 24 時間後には元の形態に復する。

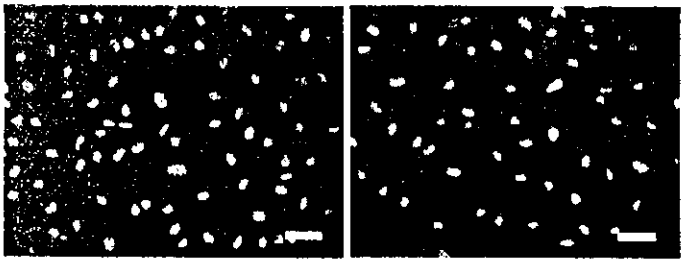

図 9　Rhodamine-phalloidin 染色アクチンフィラメント（Fアクチン）と DAPI 染色細胞核の二重染色イメージ．(左) 光化学反応前、(右)光化学反応後の活性酸素産生による顕著なFアクチン重合が観測される。Bar = 50 μm

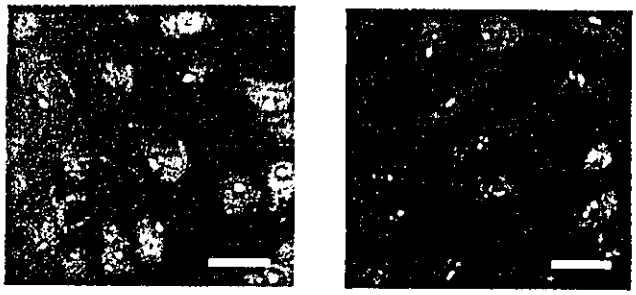

図 10　細胞間接着 tight junction 構成タンパク質 ZO-1 の免疫蛍光染色イメージ．(左) 光化学反応前、(右)光化学反応後の活性酸素産生による顕著な tight junction の喪失が観測される。Bar = 50 μm

以上のように、光化学反応の活性酸素産生による培養血管内皮細胞の形態変化は、短時間のうちに顕著に起こり、内皮下組織の露出部分に血小板の粘着凝集と白血球（好中球や単球）のローリングと接着が加速度的に誘起される。これら血管内皮細胞と血小板および白血球の粘着凝集に関して抗体を用いた接着阻害実験を試みた結果、光化学反応による急性血栓生成モデルでは、接着因子のPセレクチンとEセレクチンの関与は少ないものの、内皮細胞のトロンボモジュリン活性の減少、内皮と血小板間での接着性亢進においてVLA-2、vWFの活性化が認められ、内皮と白血球間での接着性亢進においてβ2インテグリン、ICAM-1の活性化が認められ、またCD18、CD11aの活性化による血栓生成亢進が認められた。

3．考察

脳虚血は脳血管障害のみならず心肺蘇生時や外傷時などにもみられる病態であり、脳神経細胞は虚血侵襲に極めて脆弱である。その病態・薬理作用や再潅流時の細胞・組織の機能解析を行うには、微小循環の血流動態と酸素代謝また細胞内ミトコンドリアのエネルギー代謝過程で使用されるNADH変化による虚血指標を時空間的に捉えることが極めて重要であり、本研究の多波長マルチフォトニックイメージングシステムはその要望に十分に応えるものである。光化学反応の活性酸素産生による血栓生成では、活性酸素産生、血小板 LDH 放出誘発（血小板そのものの凝集作用は抑制）、内皮細胞Fアクチン重合・細胞骨格変化、tight junction 消失、細胞質の収縮、血管内皮基底膜の露出、基底膜コラーゲンからの血小板コラーゲン受容体を介する血小板活性化、フィブリノーゲンレセプターGPⅡb/Ⅲaの活性化、vWF レセプターGPⅠbの活性化、vWFを介する接着、また白血球の活性化による二次的な活性酸素の産生、内皮基底膜の露出促進、白血球の接着性亢進、血小板の粘着亢進などが相乗的に起こる。糖尿病では非酵素的糖化反応によりGPⅠb、GPⅡb/Ⅲaの増加が顕著となり、易血栓性を示すと考えられる。微小循環障害については、上記活性酸素以外のROSや種々の活性化因子の関与についても検討する必要がある。

4．むすび

本研究では、血管炎や微小循環障害によって誘発される種々の組織傷害や細胞傷害のメカニズムを分子・細胞レベルで解析・診断するために各種蛍光・燐光標識ナノプローブと高感度イメージング技術を開発し、これらを用いて傷害の発現メカニズムと傷害からの再生・治癒過程に関する分子機序を局所的に解析した。腸間膜・肝臓・脳を対象に微小血管内の血流動態を可視化解析し、赤血球速度・変形能、血小板粘着・血栓形成過程、白血球粘着能などの動的変化を明らかにするとともに、糖尿病微小循環障害や脳虚血などの病態把握と治療効果の評価を行った。また、培養細胞系を用いて細胞内の分子機能をイメージング解析し新しい知見を得るとともに、使用したナノプローブやイメージング技術の有効性を検証した。

Microbiol. Immunol., 49(2), 181–189, 2005

Editor-Communicated Paper

Susceptibility Loci to Coronary Arteritis in Animal Model of Kawasaki Disease Induced with *Candida albicans*-Derived Substances

Toshiaki Oharaseki*[,1], Yosuke Kameoka[2], Fumiaki Kura[3], Amanda S. Persad[4], Kazuo Suzuki[4], and Shiro Naoe[1]

[1]*Department of Pathology, Ohashi Hospital, Toho University School of Medicine, Meguro-ku, Tokyo 153–8515, Japan,* [2]*Division of Genetic Resources,* [3]*Department of Bacteriology, and* [4]*Department of Bioactive Molecules, National Institute of Infectious Diseases, Shinjuku-ku, Tokyo 162–8640, Japan*

Communicated by Dr. Hidechika Okada: Received November 26, 2004. Accepted December 13, 2004

***Abstract*: We have established an animal model of coronary arteritis which is histopathologically similar to that observed in cases of Kawasaki disease (KD), is a well-known childhood vasculitis syndrome. Coronary arteritis in this mouse model has been induced by intraperitoneal injection of *Candida albicans*-derived substances (CADS). Arteritis varied by mouse strain with the highest incidence by 71.1% (27/38) found in C3H/HeN mice, but absent in CBA/JN mice (0%, 0/27), suggesting association of genomic background to develop the disease. The present study aims to elucidate the susceptibility loci associated with coronary arteritis by using this animal model. The association of the onset of arteritis with polymorphic microsatellite markers between the two strains was examined using one hundred and fifteen of N1 backcross progeny [(CBA×C3H)F1×C3H]. Based on our analysis, arteritis-susceptibility loci with suggestive linkage were mapped on *D1Mit171* and *D1Mit245* (map position 20.2 cM) on chromosome 1 (P=0.0019). These loci include several kinds of inflammatory cytokine receptors, such as interleukin 1 receptor and tumor necrosis factor receptor. We also found the cytokine response against CADS, levels of inflammatory cytokines interleukin-1β, tumor necrosis factor-α, and interleukin-6 in sera increased within 24 hr after CADS injection. Our results may indicate based on genomics that ligand-receptor interaction between these inflammatory cytokines and the receptors of these cytokines may affect the onset of arteritis.**

***Key words*: Kawasaki disease, Arteritis, *Candida albicans*, Interleukin 1 receptor, Chromosome mapping**

Kawasaki disease (KD) is an acute febrile mucocutaneous syndrome with systemic vasculitis mainly affecting infants and small children. The principal symptoms of KD are fever, congestion of ocular conjunctivae, reddening of lips and oral mucosa, swelling and reddening of palms and soles followed by peeling of skin, swelling of cervical lymph nodes coincidentally with systemic vasculitis (9). Inflammation of medium-sized muscular arteries, especially the coronary artery, is commonly associated with this disease. Ischemic heart disease with thrombotic occlusion, originating from coronary arteritis is a severe complication of KD. Histopathologically, it was reported that arteritis defined as 'productive granulomatous inflammation' was typical in KD cases (15, 19). This type of inflammation consists of dense infiltration of both neutrophils and histiocytes accompanied with a few lymphocytes. Mechanisms of developing arteritis in the patients with KD

**Address correspondence to* Dr. Toshiaki Oharaseki, Department of Pathology, Ohashi Hospital, Toho University School of Medicine, 2–17–6 Ohashi, Meguro-ku, Tokyo 153–8515, Japan. Fax: +81–3–3468–1283. E-mail: oharasek@muc.biglobe.ne.jp

Abbreviations: CADS, *Candida albicans* derived substances; cM, centi-morgan; ELISA, enzyme-linked immunosorbent assay; EvG, Elastica van Gieson; HE, hematoxylin and eosin; IFN-γ, interferon-γ; IL, interleukin; *Il1r1*, interleukin-1 receptor type 1; *Il1r2*, interleukin-1 receptor type 2; KD, Kawasaki disease; MCLS-6, mucocutaneous lymphnode syndrome-6; MPO, myeloperoxidase; MPO-ANCA, myeloperoxidase-antineutrophilic cytoplasmic antibody; PCR, polymerase chain reaction; QTL, quantitative trait of loci; TNF-α, tumor necrosis factor α; *Tnfrsf1b*, TNF receptor superfamily member 1b; *Tnfrsf8*, TNF receptor superfamily member 8; *Tnfrsf9*, TNF receptor superfamily member 9.

remain to be determined; however, there are some reports that coronary arteritis is affected by genetic polymorphism of several kinds of inflammatory cytokines, such as tumor necrosis factor α (TNF-α) (8), and interleukin-6 (IL-6) (7). Appropriate animal models of KD will allow for the clarification of the mechanisms governing the development of arteritis, and possibly, specific treatments for this disease. One of the animal models of arteritis that exist is the MRL/lpr mouse model. It is the standard animal model for studying systemic lupus erythematosus, with a common affliction to spontaneous arteritis. In MRL/lpr mice, some genes associated with arteritis have been elucidated (5). Recently, it was reported that arteritis in different tissues were under the control of different susceptibility loci (21).

Some infectious microorganisms, such as *Staphylococcus aureus* (11), *Streptococcus sanguis* (16), *Streptococcus pyogenes* (22), and *Rickettsia* (6) have been considered likely etiology candidates for this disease, though the primary causes remain unclear. These microorganisms are considered to act as the initial trigger for the development of arteritis in the patients with KD. Therefore, the initial trigger by an infectious microorganism is necessary for ideal model of KD to induce arteritis. However, this spontaneous arteritis model may not be well suited as an animal model for KD. On the other hand, Murata (13) has established a unique arteritis model that has been evaluated as an animal model of KD. In this model, arteritis induction is ascertained by injecting mice with alkaline extract of *Candida albicans* as an experimental arteritis. It should be noted that the quantity of this yeast was observed to be in elevated in stool samples of KD patients (14). The histology of this experimental arteritis model is similar to that of an autopsy case of KD (2). In this model, genetics in mice may have an influence on the development of arteritis. It was shown that the incidence of coronary arteritis varied by mouse strain, with the C3H/HeN mice having the highest incidence and coronary arteritis being absent in CBA/JN strains (20).

To identify susceptibility loci to the coronary arteritis, we analyzed coronary arteritis in [(CBA/JN×C3H/HeN)×C3H/HeN]N1 backcross progeny. The evidence presented herein shows that the susceptibility loci are linked to genes of several inflammatory cytokine receptors found in the coronary artery.

Materials and Methods

Chemicals. Sabouraud-2% dextrose broth (MERCK, Darmstadt, Germany) was used as culture medium. Sodium chloride, potassium hydroxide, acetic acid, ethanol, acetone, diethyl ether (Wako Pure Chemical Industries, Ltd., Osaka, Japan) and *n*-octyl alcohol (Kanto Chemical Co., Tokyo) were used for polysaccharide extraction from the cell wall of *C. albicans*.

Genomic DNA was isolated from whole blood obtained from the tail of animals using the QIAamp DNA mini kit (Qiagen, Hilden, Germany). FAM labeled primers for microsatellite markers were purchased from SIGMA Genosys Japan (Ishikari, Japan). Amplification and labeling of each microsatellite locus were performed by using Z-*Taq* polymerase (TaKaRa, Kyoto, Japan).

Animals. Mice, CBA/JNCrj (CBA/JN) and C3H/HeNCrj (C3H/HeN), were purchased from Charles River Japan (Astugi, Japan). Using C3H/HeN and CBA/JN strains, (C3H/HeN female×CBA/JN male)F1, (CBA/JN female×C3H/HeN male)F1, and [(CBA/JN×C3H/HeN)F1×C3H/HeN]N1 were prepared. N1 backcross progeny, 4-week-old males, were used for the linkage analysis (n=115). These mice were housed in a specific pathogen-free animal quarter and cared for under strict ethical guidelines.

Preparation of alkaline extract of C. albicans *(CADS).* CADS were prepared as follows. *C. albicans* (strain MCLS-6) isolated from the feces of patients with typical Kawasaki disease, was cultured in Sabouraud's dextrose medium with 2% glucose at 37 C. After a 72-hr incubation period, the yeast was harvested by centrifugation and extracted sequentially with boiling water, 0.1 M, and 0.5 M potassium hydroxide. After neutralization with acetic acid and dialysis against distilled water for 3 days, the extract was precipitated with ethanol. Four milligrams of the CADS, suspended in 0.2 ml of phosphate-buffered saline without calcium and magnesium (PBS(−)), were prepared as the inoculants.

Experimental schedule. Inoculation was conducted as described in the previous procedures (13). Namely, mice were injected once daily with 0.2 ml of inoculate intraperitoneally for 5 consecutive days during the first and fifth week. Each mouse was sacrificed with carbon dioxide asphyxiation at the ninth week and autopsied.

Histopathological evaluation of arteritis. The following visceral organs were obtained for histopathological examination: heart, aorta, kidney, lung, liver, pancreas, spleen, thymus, testis, muscle of hind leg, and spine. These specimens were fixed in 10% formalin and embedded in paraffin. Hematoxylin and eosin (HE) and Elastica van Gieson (EvG) stains were performed by routine histological techniques. Arteritis in individual mice was determined using light microscopy. A mouse with inflammation involving all layers of coronary artery and/or the aortic root was considered positive for coronary arteritis and used for linkage analysis.